An ultra-high-affinity small organic ligand of fibroblast activation protein for tumor-targeting applications

Jacopo Millul[a,1], Gabriele Bassi[a,1], Jacqueline Mock[b,1], Abdullah Elsayed[b], Christian Pellegrino[b], Aureliano Zana[a], Sheila Dakhel Plaza[a], Lisa Nadal[a], Andreas Gloger[a], Eleonore Schmidt[a], Ilaria Biancofiore[a], Etienne J. Donckele[a], Florent Samain[a], Dario Neri[b,c,2], and Samuele Cazzamalli[a,2]

[a]Philochem AG, R&D department, CH-8112 Otelfingen, Switzerland; [b]Swiss Federal Institute of Technology, Department of Chemistry and Applied Biosciences, CH-8093 Zurich, Switzerland; and [c]Philogen S.p.A., 53100 Siena, Italy

Edited by Robert Langer, Massachusetts Institute of Technology, Cambridge, MA, and approved March 15, 2021 (received for review January 29, 2021)

We describe the development of OncoFAP, an ultra-high-affinity ligand of fibroblast activation protein (FAP) for targeting applications with pan-tumoral potential. OncoFAP binds to human FAP with affinity in the subnanomolar concentration range and cross-reacts with the murine isoform of the protein. We generated various fluorescent and radiolabeled derivatives of OncoFAP in order to study biodistribution properties and tumor-targeting performance in preclinical models. Fluorescent derivatives selectively localized in FAP-positive tumors implanted in nude mice with a rapid and homogeneous penetration within the neoplastic tissue. Quantitative in vivo biodistribution studies with a lutetium-177–labeled derivative of OncoFAP revealed a preferential localization in tumors at doses of up to 1,000 nmol/kg. More than 30% of the injected dose had already accumulated in 1 g of tumor 10 min after intravenous injection and persisted for at least 3 h with excellent tumor-to-organ ratios. OncoFAP also served as a modular component for the generation of nonradioactive therapeutic products. A fluorescein conjugate mediated a potent and FAP-dependent tumor cell killing activity in combination with chimeric antigen receptor (CAR) T cells specific to fluorescein. Similarly, a conjugate of OncoFAP with the monomethyl auristatin E-based Vedotin payload was well tolerated and cured tumor-bearing mice in combination with a clinical-stage antibody-interleukin-2 fusion. Collectively, these data support the development of OncoFAP-based products for tumor-targeting applications in patients with cancer.

tumor targeting | small molecule therapeutics | FAP

Small organic ligands which selectively bind with high affinity to tumor-associated antigens are increasingly applied as targeting delivery vehicles of small payloads such as radionuclides (1, 2), drugs (3–5), and fluorophores (6, 7) to tumor sites. In principle, the use of small ligands for targeting applications offers several advantages compared to intact immunoglobulins, including superior penetration of solid neoplastic lesions (8), lower immunogenicity (9), and a reduced cost of goods (10). Low molecular weight compounds may reach their target in vivo in a matter of seconds, thanks to rapid extravasation after intravenous administration (8). A strikingly selective accumulation of small ligands in neoplastic masses has been demonstrated for a small number of targets including somatostatin receptor type 2 (SSTR-2) (11), prostate-specific membrane antigen (PSMA) (12), and carbonic anhydrase IX (CAIX) (13), for which high-affinity small organic ligands are available. Those ligands are typically specific for defined tumor entities, such as neuroendocrine tumors (11), prostate cancer (3), and clear cell renal cell carcinoma (2).

^{177}Lu-DOTATATE (Lutathera), a small-molecule product targeting SSTR-2, has been approved based on phase III data in which a clinically meaningful 82% reduction in the risk of disease progression or death was demonstrated in patients with gastroenteropancreatic neuroendocrine tumors (GEP-NETs) (14). Similar data are expected from the currently ongoing phase III VISION trial for ^{177}Lu-PSMA-617 (clinical trial no. NCT03511664), a radiolabeled small molecule that binds with high affinity to PSMA and that enables targeted beta particle therapy in metastatic castration-resistant prostate cancer patients (15). PHC-102, a ^{99m}Tc-labeled small-molecule derivative targeting CAIX, exhibited favorable uptake in primary and metastatic lesions in patients with renal cell carcinoma (RCC) (2). In light of the promising performance of small organic ligands, it would be desirable to discover and develop small molecules with a broader tumor-targeting potential, therefore covering multiple cancer types.

Fibroblast activation protein (FAP) is a type II integral membrane serine protease which is abundantly expressed in the stroma of more than 90% of the epithelial cancers, including malignant breast, colorectal, skin, prostate, and pancreatic cancers (16, 17), while exhibiting a restricted expression in normal adult tissues (18, 19). Haberkorn and coworkers (1, 20, 21) have recently described a series of FAP ligands capable of selective accumulation in FAP-positive tumors in mice and in patients. One of these products (named FAPI-04) showed impressive tumor to background ratios at early time points (i.e., few hours after administration) in a broad range of different cancer types in patients. More than 28 tumor

Significance

Fibroblast activation protein (FAP) has recently emerged as a tumor-associated antigen with abundant and selective expression in the majority of human solid malignancies. To the best of our knowledge, OncoFAP is the highest-affinity small organic FAP ligand reported to date, with a dissociation constant of 680 pM, as measured by fluorescence polarization. Upon intravenous administration, both fluorescent and radiolabeled OncoFAP derivatives exhibited a rapid and selective accumulation in FAP-positive tumors, sparing normal tissues. OncoFAP was also used as a modular component for the generation of therapeutic products, enabling the targeted delivery of a potent beta-emitter (lutetium-177), of fluorescein-specific chimeric antigen receptor (CAR) T cells or of highly cytotoxic auristatin derivatives to FAP-positive tumors in vitro and in vivo.

Author contributions: D.N. and S.C. designed research; J. Millul, G.B., J. Mock, A.E., C.P., E.J.D., F.S., and S.C. performed research; J. Millul, G.B., A.E., A.Z., S.D.P., L.N., A.G., E.S., I.B., E.J.D., and F.S. contributed new reagents/analytic tools; J. Millul, G.B., J. Mock, and S.C. analyzed data; and J. Millul, G.B., J. Mock, D.N., and S.C. wrote the paper.

Competing interest statement: D.N. is a cofounder and shareholder of Philogen (http://www.philogen.com/en/), a Swiss-Italian Biotech company that operates in the field of ligand-based pharmacodelivery. J. Millul, G.B., J. Mock, A.Z., S.D.P., L.N., A.G., E.S., I.B., E.J.D., F.S., and S.C. are employees of Philochem AG, the daughter company of Philogen, acting as the discovery unit of the group.

This article is a PNAS Direct Submission.

[1]J. Millul, G.B., and J. Mock contributed equally to this work.

[2]To whom correspondence may be addressed. Email: neri@pharma.ethz.ch or samuele.cazzamalli@philochem.ch.

This article contains supporting information online at https://www.pnas.org/lookup/suppl/doi:10.1073/pnas.2101852118/-/DCSupplemental.

Published April 13, 2021.

types including breast, lung, pancreatic, head and neck, esophagus, and colorectal cancer presented a remarkably high uptake of a FAP-targeted small molecule labeled with gallium-68 (1, 20, 21). For this reason, FAP has recently been dubbed as "the next billion-dollar target for theranostic products" (22).

Here, we describe how the chemical modification of a quinoline moiety in position 8 led to the discovery of OncoFAP, a small organic FAP ligand with a dissociation constant in the subnanomolar concentration range. OncoFAP exhibited a strikingly selective and efficient tumor-targeting performance when equipped with various types of payloads, including radionuclides, fluorophores, and cytotoxic drugs. The targeting delivery of radionuclides to solid tumors is rapidly gaining in popularity, as it may open theranostic opportunities, associated with the use of gallium-68 for positron emission tomography (PET) imaging and of lutetium-177 for therapeutic applications (23). The delivery of fluorescein to tumors enables the conditional activation of chimeric antigen receptor (CAR) T cells, which display a potent biocidal activity only in the presence of fluorescein-labeled adaptor molecules specific to a tumor antigen (24, 25). Finally, small-molecule–drug conjugates (SMDCs) promise to represent a valid alternative to antibody–drug conjugates for cancer therapy, with better tumor penetration and a lower cost of goods (8, 26, 27).

Results

Synthesis of OncoFAP Ligand and Its Derivatives. The OncoFAP ligand was produced as pure material following the synthetic scheme presented in Fig. 1*A* (compound **1**). OncoFAP presents a carboxylic acid moiety that can be functionalized with various payloads using amide coupling methodologies obtaining compounds **2**, **3**, **4**, and **5** (Fig. 1*B*). Detailed synthetic procedures are presented in *SI Appendix*. Compound **2** presents a fluorescein payload and was used to assess binding to human and murine FAP antigen. Compound **3** presents an Alexa 488 payload and was used to assess in vivo penetration in tumor-bearing mice. Compound **4** presents a (1-(1,3-carboxy-propyl)-4,7,10(carboxymethyl)-1,4,7,10 tetraazacyclo-dodecane (DOTAGA) function that can be radiolabeled with lutetium-177 and used to assess in vivo quantitative biodistribution in tumor-bearing mice. OncoFAP-vedotin (compound **5**) includes a linker payload therapeutic module composed of a cleavable valine–citrulline linker, a para-aminobenzyl carbamate self-immolative moiety, and a potent cytotoxic monomethyl auristatine E (MMAE) payload.

Characterization of OncoFAP Binding to Human and Murine FAP. The possibility to form a stable complex between OncoFAP and the target antigen was tested by coincubating recombinant human and murine FAP with OncoFAP-fluorescein (compound **2**) and by loading the mixture onto a desalting PD-10 column run by gravity. Compound **2** elution was followed by monitoring fluorescence intensity at 485 nm (excitation wavelength), while protein concentration was estimated on the basis of the absorbance at 280 nm. OncoFAP-fluorescein coeluted with both murine and human FAP, therefore confirming formation of a stable complex after coincubation in solution (Fig. 1*C*).

The binding affinity for human and for murine FAP of compound **2** was measured by fluorescence polarization (Fig. 1*D*). Compound **2** showed ultra-high affinity toward the two isoforms of the protein target ($K_{D,humanFAP}$ = 0.68 nM; $K_{D,murineFAP}$ = 11.6 nM). OncoFAP (compound **1**) was additionally evaluated as an inhibitor of FAP in an enzymatic assay in the presence of the Z-Gly-Pro-AMC substrate (Fig. 1*E*). OncoFAP potently inhibited the enzymatic activity of both murine and human FAP isoforms ($IC_{50,humanFAP}$ = 16.8 nM, $IC_{50,murineFAP}$ = 14.5 nM).

Ligand Internalization Analysis on Tumor Cells Expressing FAP. Wild-type (wt) SK-RC-52 and HT-1080 tumor cells were transduced with transmembrane human FAP (hFAP) using lentiviral particles. Tumor cells expressing hFAP on the membrane were isolated by fluorescence-activated cell sorting (FACS) after transduction. FAP expression was confirmed by flow cytometry analysis on SK-RC-52.hFAP and HT-1080.hFAP cells after sorting (Fig. 2).

Confocal microscopy experiments were performed in order to investigate the internalization of OncoFAP derivatives upon ligand binding to human FAP on the membrane of cancer cells. OncoFAP-fluorescein (compound **2**) was incubated on living adherent SK-RC-52.hFAP and HT-1080.hFAP cancer cells (expressing high levels of the FAP antigen on their surface) that were imaged after incubation for 1 h (Fig. 2). Compound **2** showed selective accumulation on the membrane of SK-RC-52.hFAP cancer cells. OncoFAP binding to FAP was not followed by endocytosis and receptor-mediated internalization on this cell line (Fig. 2*A*). In strong contrast to the results obtained on SK-RC-52.hFAP cells, OncoFAP-fluorescein efficiently internalized in HT-1080.hFAP cells (Fig. 2*B*). In control experiments, compound **2** did not show interaction with FAP-negative SK-RC-52.wt and HT-1080.wt cells.

In Vivo Tumor and Organ Penetration Analysis of OncoFAP. In order to understand the microscopic distribution of OncoFAP-based targeted conjugates in solid lesions and healthy tissues, OncoFAP-Alexa488 (compound **3**) was intravenously administered to athymic Balb/c AnNRj-Foxn1 mice bearing subcutaneous SK-RC-52.hFAP and HT-1080.hFAP tumors in their right flank. FAP-negative SK-RC-52.wt tumors were implanted in the left flank of the animals and served as the negative control for the experiment. OncoFAP-Alexa488 selectively accumulated in FAP-positive tumors with a homogeneous distribution over the solid lesions 1 h after administration of the compound (Fig. 3 *A* and *B*). No significant accumulation of OncoFAP-Alexa488 was observed in FAP-negative tumors and in healthy organs. Additional biodistribution experiments performed with a fluorescent OncoFAP-IRdye750 derivative in tumor-bearing mice confirmed selective localization of the compound to FAP-positive tumors (*SI Appendix*, Fig. S1).

Quantitative Biodistribution of ^{177}Lu-OncoFAP in Tumor-Bearing Mice. In order to assess the in vivo tumor-targeting performance of OncoFAP derivatives, a quantitative biodistribution study with a lutetium-177 radiolabeled preparation of the ligand was performed in athymic Balb/c AnNRj-Foxn1 mice bearing SK-RC-52.hFAP renal cell carcinoma. The OncoFAP-DOTAGA (compound **4**) was radiolabeled with lutetium-177 as described in Fig. 4*A*, with full incorporation of the radiometal confirmed by radio-HPLC (high-performance liquid chromatography) analysis (*SI Appendix*). ^{177}Lu-OncoFAP was injected at the dose of 50 nmol/kg and animals were euthanized 10 min, 1, 3, or 6 h after intravenous administration. ^{177}Lu-OncoFAP accumulated selectively in the tumor already 10 min after injection (32% injected dose [ID]/g), with a sustained uptake (i.e., higher than 20% ID/g) in the lesions over the first 6 h time window. The highest tumor to blood (116:1) and tumor to kidney (33:1) ratio were observed 3 h after intravenous injection (Fig. 4*B*). In a separate biodistribution experiment in the SK-RC-52.hFAP model, ^{177}Lu-OncoFAP was injected at increasing doses from 125 nmol/kg to 1 μmol/kg, and the uptake in tumors and healthy tissues was analyzed 3 h after intravenous administration. A dose-dependent accumulation in SK-RC-52.hFAP tumors was observed with a target saturation observable at doses higher than 500 nmol/kg (Fig. 4*C*).

Universal CAR T Cell Killing Assay. OncoFAP-fluorescein (compound **2**) was applied as a cross-linker to mediate cancer cell lysis by universal CAR T cells (UniCAR T cells), engineered to recognize the payload through the expression of a specific anti-fluorescein CAR on their surface (Fig. 5*A*). The killing efficacy was assessed by flow cytometry on both SK-RC-52.hFAP and on

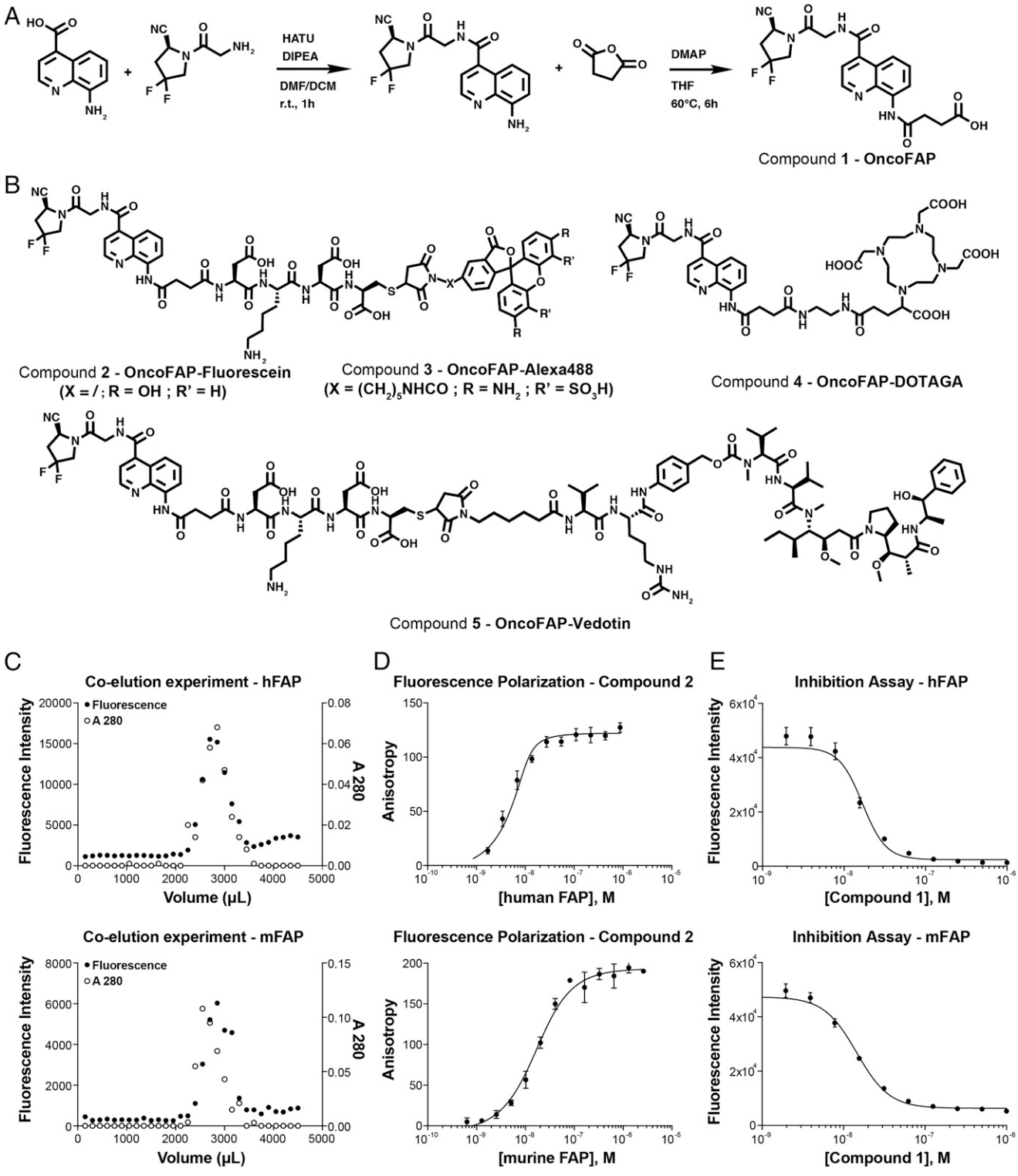

Fig. 1. (*A*) Synthesis of the precursor of small-molecule FAP-targeting derivatives of OncoFAP (compound **1**). The ligand features a di-fluoro-cyano-proline, an 8-amido-quinoline ring, and a carboxylic acid, which can be used as portable conjugation moiety of various payloads. (*B*) The chemical structures of OncoFAP-fluorescein (compound **2**), OncoFAP-Alexa488 (compound **3**), OncoFAP-DOTAGA (compound **4**), and OncoFAP-vedotin (compound **5**) derivatives. (*C*) The coelution experiments performed with OncoFAP-fluorescein conjugate (compound **2**). OncoFAP-fluorescein forms a stable complex both with recombinant hFAP and mFAP. (*D*) The affinity of OncoFAP for hFAP and mFAP was measured by fluorescence polarization. OncoFAP showed ultra-high affinity for the two isoforms of the FAP target ($K_{D,humanFAP}$ = 0.68 nM, $K_{D,murineFAP}$ = 11.6 nM). (*E*) The enzymatic assay performed with OncoFAP (compound **1**). OncoFAP potently inhibited the enzymatic activity of hFAP and mFAP ($IC_{50,humanFAP}$ = 16.8 nM, $IC_{50,murineFAP}$ = 14.5 nM).

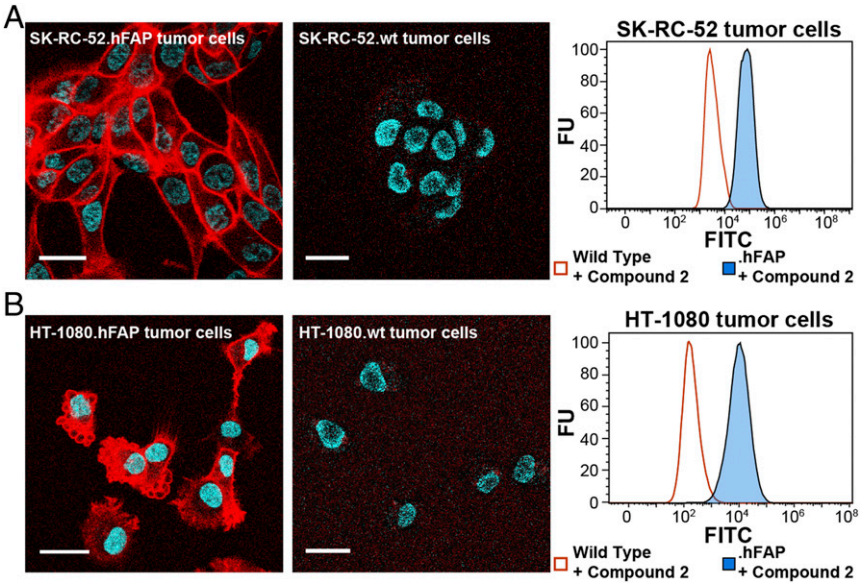

Fig. 2. (*A*) Confocal microscopy images and flow cytometry analysis after exposure to OncoFAP-fluorescein (compound **2**) on FAP-expressing SK-RC-52 and (*B*) HT-1080 cells. OncoFAP-fluorescein was mainly bound to the SK-RC-52.hFAP cell surface showing lack of internalization. In contrast, HT-1080.hFAP cells efficiently internalized OncoFAP-fluorescein. Flow cytometry analysis on SK-RC-52.hFAP and HT-1080.hFAP confirms binding of compound **2** to both tumor cell lines. No interaction with HT-1080.wt and SK-RC-52.wt was observed in confocal microscopy and flow cytometry experiments (negative controls). Red = fluorescein derivatives staining; blue = Hoechst 33342 staining. FU = relative fluorescence unit. (Scale bar, 25 μm.)

HT-1080.hFAP tumor cells. The tumor cells were incubated with escalating concentrations of compound **2** in the presence of UniCAR T cells (effector to target ratio of 1:1). A dose-dependent killing of SK-RC-52.hFAP cells could be observed, with saturation obtained at concentrations of OncoFAP-fluorescein above 1 nM (Fig. 5*A*). Interestingly, when tested in an internalizing scenario on HT-1080.hFAP cells (Fig. 2*B*), OncoFAP-fluorescein could not mediate UniCAR T cell–dependent killing at any of the concentrations tested in the experiment (Fig. 5*C*).

Therapy Experiment with OncoFAP-Vedotin in Combination with L19-IL2 in Tumor-Bearing Mice. The anticancer efficacy of OncoFAP-vedotin (compound **5**) as monotherapy and in combination with L19-IL2 was assessed in athymic Balb/c AnNRj-Foxn1 mice bearing SK-RC-52.hFAP renal cell carcinoma. OncoFAP-vedotin was intravenously administered at 500 nmol/kg, as this dose was considered safe based on a preliminary dose escalation experiment presented in *SI Appendix*, Fig. S2. L19-IL2 was administered at 2.5 mg/kg, a dose that has been previously described as nontoxic and efficacious when the product is combined with MMAE-based SMDCs (28). Therapy experiments started when the average volume of established tumors had reached 100 mm^3. Compounds were administered following the schedule indicated in Fig. 6*A*. A potent in vivo anticancer activity was observed when OncoFAP-vedotin was administered as a single agent. The combination of the OncoFAP-drug conjugate with L19-IL2 enhanced the antitumor activity of the drug and induced complete and durable cures in all animals treated (Fig. 6*A*). The administration of OncoFAP-vedotin, L19-IL2, and their combination was well tolerated, with no sign of acute toxicity observed after injection of the products (Fig. 6*B*).

Discussion

We have described a novel ligand specific to FAP (termed OncoFAP), with potency in the subnanomolar concentration range. Derivatives of OncoFAP were shown to preferentially localize to FAP-positive tumors and to display an anticancer activity in vitro and in vivo.

FAP has been considered as a target for antibody-based pharmacodelivery activities for over two decades (29–31), but nuclear medicine imaging results based on intact antibodies have been rather disappointing (32, 33). Industrial attempts to use anti-FAP immunoglobulins for the development of antibody–drug conjugates have led to encouraging results in some mouse models of cancer (34). However, similar beneficial effects could not be observed by using antibody-based therapeutics directed against FAP (31). The field of ligand-based FAP targeting has been revolutionized by the pioneering work of Haberkorn and coworkers, who have explored a series of small-molecule FAP binders for nuclear medicine applications. One of those ligands (termed FAPI-04) has shown encouraging results in quantitative biodistribution experiments in tumor-bearing mice and excellent selectivity in PET studies in cancer patients using gallium-68 as a radionuclide (1, 20, 21, 35). More than 30 different tumor types could be efficiently imaged using FAPI-04, which has led to intense industrial developments in the field (1, 22).

The use of small molecules as tumor-targeting agents, in alternative to conventional antibodies, is gaining momentum. The small size of organic ligands typically translates into faster extravasation and deeper penetration into the tumor mass compared to immunoglobulins (8). Moreover, organic products are cheaper and faster to produce compared to antibodies. However, it is becoming increasingly clear that a selective tumor accumulation with small molecules can only be achieved if ligands bind with ultra-high affinity (i.e., K_D below 10 nM) against a cognate target, which is abundant, accessible, and selective (36, 37). In comparative binding studies, OncoFAP bound to FAP with a K_D of 0.68 nM, while a fluorescent derivative of FAPI-04 displayed a K_D of 1.02 nM (*SI Appendix*, Fig. S3). Moreover, OncoFAP exhibited a better cross-reactivity with the mouse antigen, which may facilitate preclinical experiments (*SI Appendix*, Fig. S3).

There is a growing interest in the use of small tumor-targeting agents equipped with therapeutic radionuclides for cancer treatment. A lutetium-177 somatostatin analog (Lutathera) has recently gained marketing authorization for the treatment of neuroendocrine tumors, while a lutetium-177–labeled PSMA ligand is in

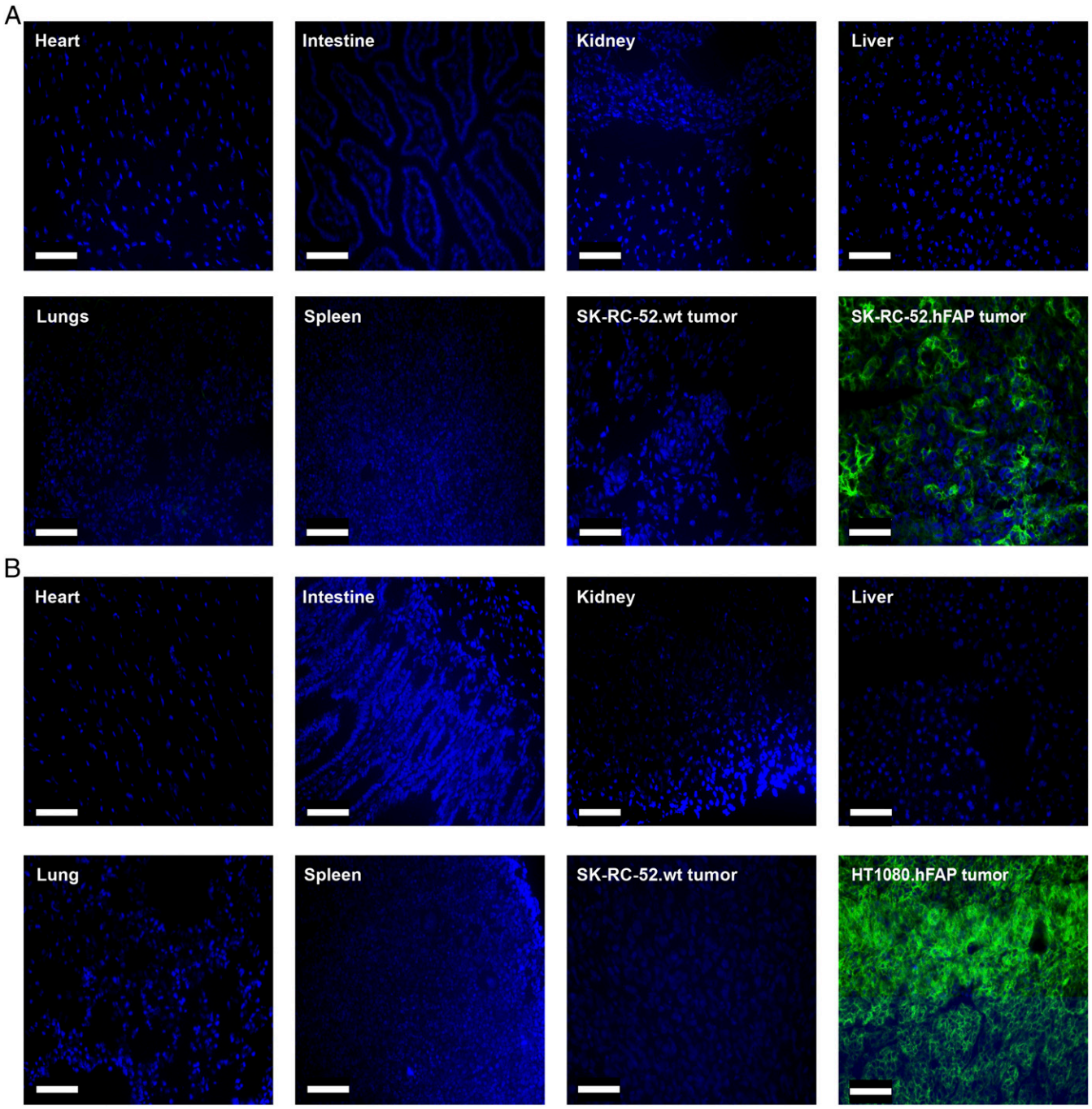

Fig. 3. (*A*) Ex vivo biodistribution in mice bearing SK-RC-52.hFAP or HT-1080.hFAP (*B*) as antigen-positive tumors and SK-RC-52.wt as an antigen-negative tumor 1 h after the intravenous injection of 40 nmol of targeted dye conjugate **3**. In both cases, the compound selectively localized to the tumor while being undetectable in all healthy organs analyzed. Green = OncoFAP-Alexa488, blue = nucleus. (Scale bar, 100 μm.)

advanced phase III studies for the treatment of metastatic prostate cancer. OncoFAP labeled with lutetium-177 has shown favorable biodistribution results in tumor-bearing mice. If imaging and dosimetric studies in humans (which are ongoing) are successful, it may be conceivable to use that product for the targeted radionuclide therapy of patients who score positive at PET imaging and do not have therapeutic alternatives.

A fluorescein conjugate of OncoFAP redirected the biocidal activity of universal CAR T cells against FAP-positive tumor cell lines. Interestingly, the approach worked better with SK-RC-52.hFAP cells (which do not internalize the FAP antigen) compared to HT-1080-hFAP cells (which show an almost complete ligand internalization within minutes) (Figs. 2 and 5). In cancer patients, FAP is frequently found in the tumor stroma (19), and it remains to be seen whether CAR T cell–based approaches may work against a stromal target. Encouraging results have recently been reported for CAR T cells against a different stromal antigen (the alternatively spliced extra-domain B domain of fibronectin) (38). The use of universal CAR T cells, specific against fluorescein, together with small bispecific adaptors may be preferable to conventional CAR T cells, as the tumor-killing activity can be modulated by the fast clearance of small molecules

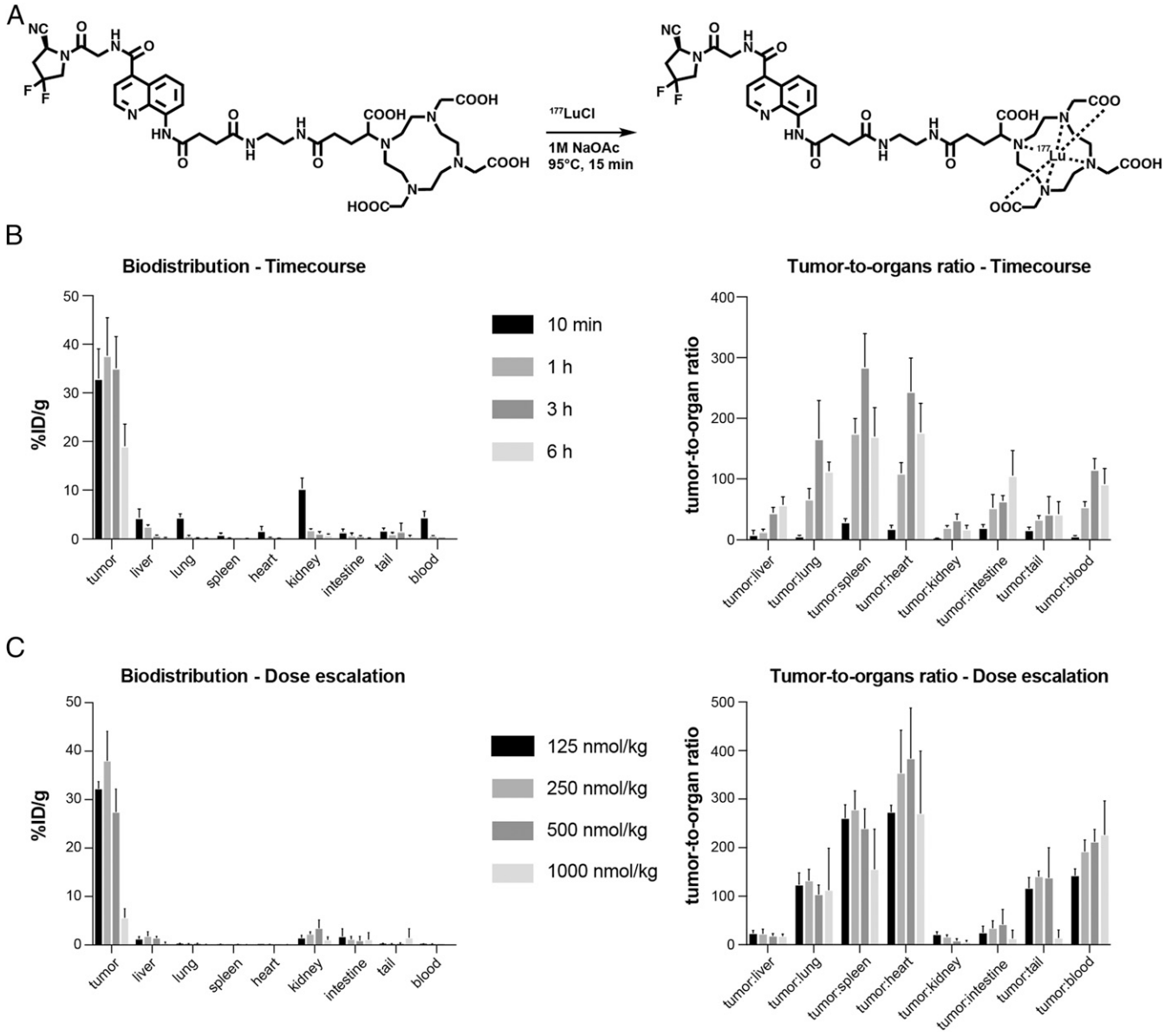

Fig. 4. (*A*) Radiolabeling scheme of OncoFAP-DOTAGA (compound **4**) with lutetium-177 to obtain ^{177}Lu-OncoFAP. Compound **4** includes an ultra-high-affinity FAP-targeting ligand and a DOTAGA chelator, which efficiently incorporates the lutetium-177 radionuclide. (*B*) The quantitative biodistribution of ^{177}Lu-OncoFAP (radiolabeled compound **4**) at different time points after intravenous administration (56.7 μg/kg, 50 nmol/kg) in SK-RC-52.hFAP tumor-bearing mice. The ligand accumulated selectively in FAP-positive tumors, reaching maximum uptake values in lesions 1 h after administration. (*C*) The quantitative biodistribution analysis of radiolabeled lutetium-177–compound **4** after intravenous injection of different doses at 3 h postinjection. Doses between 125 and 500 nmol/kg gave excellent tumor uptake and tumor to organ ratios.

serving as a "bridge" between the engineered T cell and the tumor (24, 25, 39).

We have observed a potent antitumor activity in mice using a conjugate of OncoFAP with vedotin, the linker payload moiety used in Adcetris, Padcev, and Polivy (approved anticancer antibody–drug conjugates) (40–42). The findings are in keeping with previous reports of our group in which we used small ligands specific to CAIX for the construction of SMDCs (4, 8, 28). SMDCs directed against FAP and against CAIX displayed potent and selective activity against antigen-positive tumor cells. In our hands, cancer cures could routinely be achieved when SMDCs were combined with antibody–interleukin-2 conjugates (e.g., L19-IL2), which boost the action of natural killer cells against damaged tumor cells (4, 43). SMDCs specific to the folate receptor and to PSMA have previously been investigated in preclinical studies and in clinical trials (clinical trials no. NCT01170650 and NCT02202447) (44, 45). More recently, the use of bicyclic peptide-drug conjugates has shown encouraging results in mouse models of cancer, which has led to the initiation of clinical trials (NCT03486730) (26). Collectively, these data suggest that small-molecule ligands may serve as valuable agents for the pharmacodelivery of potent cytotoxic drugs. Emerging experimental evidence suggests that a potent anticancer activity may be observed also in the absence of ligand internalization, provided that suitable linker-payloads are used, which can be cleaved in the neoplastic extracellular environment (4).

The versatile functionalization of OncoFAP and the favorable biodistribution results observed in tumor-bearing mice (with excellent tumor to organ ratios as early as 10 min after intravenous administration) (Fig. 4) suggest that this ligand may serve as a platform for the development of therapeutic agents and of

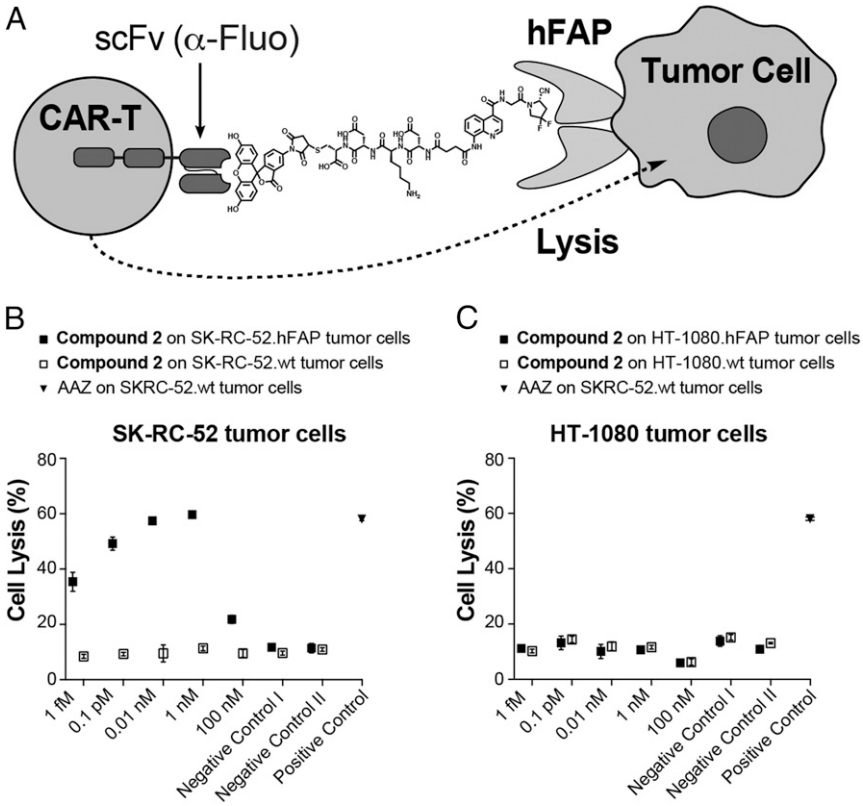

Fig. 5. (*A*) Representation of the immunological synapse of a fluorescein-specific universal CAR T cell with a FAP-expressing tumor cell, established by cross-linking the cells with the OncoFAP-fluorescein heterobifunctional adaptor (compound **2**). Results of the in vitro killing assay of (*B*) SK-RC-52.hFAP and (*C*) HT-1080.hFAP tumor cells. Killing is given as a function of compound **2** concentration and monitored 24 h after coincubation of UniCAR T cells, the OncoFAP-fluorescein adaptor, and tumor cells. SK-RC-52.wt and HT-1080.wt (wild-type FAP-negative cells) are used throughout the experiment as control cell lines to demonstrate the correlation between antigen expression and killing by UniCAR T cells. Negative control I = nontransduced T cells (no CAR expression) on tumor cells with compound **2** (1 nM). Negative control II = UniCAR T cells on tumor cells with compound **1** (1 nM). Positive control = UniCAR T cells on SK-RC-52 tumor cells with acetazolamide-fluorescein (1 nM).

companion diagnostics. The results of PET imaging studies using a ^{68}Ga-labeled OncoFAP derivative (which are ongoing) will be crucially important in order to show which tumor types are preferably suited for FAP-based targeting strategies. As OncoFAP works with different types of payloads, a comparative evaluation of performance in clinical studies may shed light on the relative advantages of different approaches, such as radionuclide therapy, drug delivery, universal CAR T cells, and possibly, the generation of small-molecule–based bispecifics.

Materials and Methods

Detailed synthetic procedures and characterization of the presented compounds (i.e., HPLC purity of final products and mass spectrometry data) are described in *SI Appendix* together with the detailed production procedures and characterization of the presented proteins (i.e., amino acid sequences, sodium dodecyl sulfate–polyacrylamide gel electrophoresis [SDS-PAGE], and size-exclusion chromatography [SEC] data), production of lentiviral particles used for transduction of tumor cell lines, additional in vivo results, and the FACS gating strategy for the UniCAR T cell killing assay.

Cloning, Expression, and Biochemical Characterization of hFAP and Murine FAP. The extracellular domain (ECD) of hFAP and of murine FAP (ECD mFAP) genes were cloned into the mammalian cell expression vector pcDNA3.1(+) (Invitrogen) using NheI/NotI restriction sites. The proteins were expressed by transient gene expression in CHO-S cells and purified to homogeneity via Ni-NTA Agarose resin (Roche) chromatography. Purified hFAP was dialyzed into Hepes buffer (100 mM NaCl and 50 mM Hepes, pH 7.4). The quality of the proteins was assessed by SDS-PAGE and by SEC on a Superdex 200 Increase 10/300 GL column on an ÄKTA Fast Protein Liquid Chromatograph (GE Healthcare). The amino acidic sequences are described in *SI Appendix*, Figs. S3 and S4.

Coelution Experiments of Ligand–Protein Complexes. PD-10 columns were preequilibrated with running buffer (50 mM Tris, 100 mM NaCl, and 1 mM ethylenediaminetetraacetic acid [EDTA], pH = 7.4). Proteins (hFAP = 2 μM, mFAP = 5 μM) were preincubated with compound **2** (100 nM), loaded on the column, and flushed with running buffer. Fractions of the flow through (150 μL) were collected in 96-well plates, and the fluorescence intensity associated with the concentration of compound **2** was measured immediately on a Tecan microtiter plate reader (excitation wavelength = 485 nm, emission wavelength = 535 nm). The concentration of the proteins in different fractions was estimated by measuring the absorbance at 280 nm.

Affinity Measurement to hFAP and mFAP by Fluorescence Polarization. Fluorescence polarization experiments were performed in 384-well plates (nonbinding, ps, f-bottom, black, high volume, 30 μL final volume). Stock solutions of hFAP (4 μM) and mFAP (5 μM) were serially diluted with buffer (50 mM Tris, 100 mM NaCl, and 1 mM EDTA, pH = 7.4), while the final concentration of the binders was kept constant at 10 nM. The fluorescence anisotropy was measured on a Tecan microtiter plate reader. Experiments were performed in triplicate, and the mean anisotropy values were fitted using Prism 7 ((Y = m1 + m2 × 0.5 × ((X + k + m3) − sqrt((X + k + m3)^2 − 4 × X × k)), where k is the concentration of the fluorescent binder).

In Vitro Inhibition Assay on hFAP and mFAP. Enzymatic activity of hFAP and mFAP on the Z-Gly-Pro-AMC substrate was measured at room temperature on a microtiter plate reader, monitoring the fluorescence at an excitation wavelength of 360 nm and an emission wavelength of 465 nm. The reaction mixture contained substrate (20 μM), protein (20 nM, constant), assay buffer (50 mM Tris, 100 mM NaCl, and 1 mM EDTA, pH = 7.4), and compound **1**

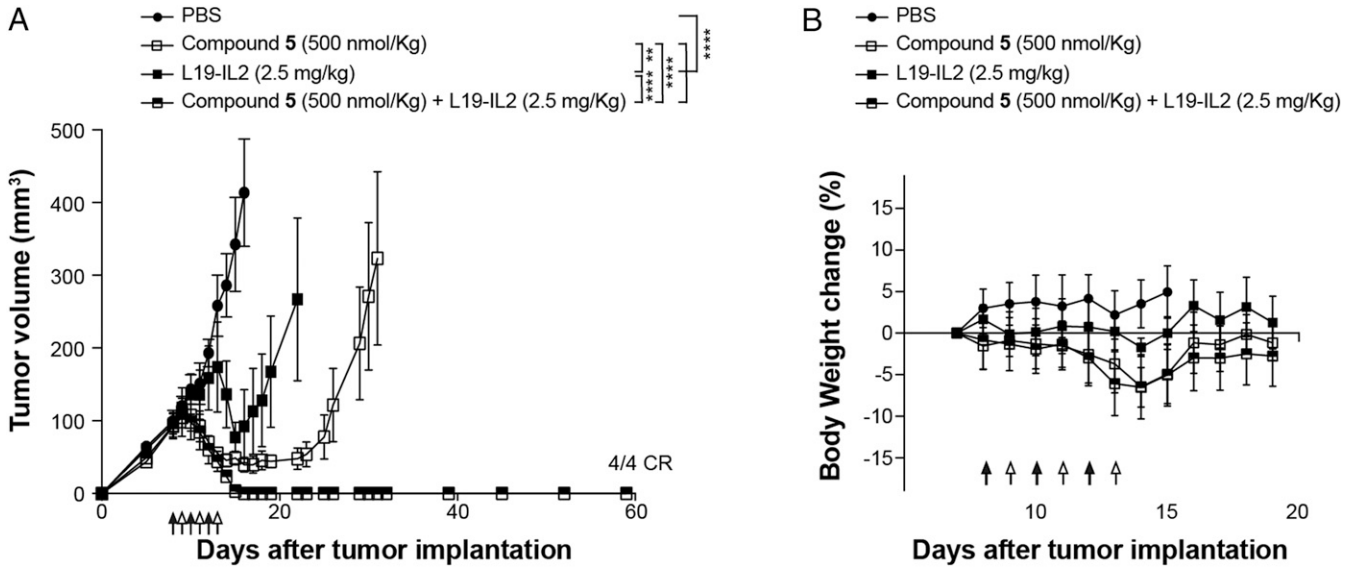

Fig. 6. (*A*) Therapeutic activity of OncoFAP-vedotin (compound **5**) as a single agent and in combination with L19-IL2 in BALB/c nu/nu mice bearing SK-RC-52.hFAP tumors. The efficacy of the different treatments is assessed by daily measurement of tumor volume (mm^3) during and after administration of the drugs. Data points represent mean tumor volume ± SEM ($n = 4$ per group). Animals were treated with OncoFAP-vedotin (compound **5**; 500 nmol/kg; IV; black arrow) and L19-IL2 (2.5 mg/kg; IV; white arrow) as monotherapy or in a combination regimen following the schedule depicted in the figure. When given as single agent, OncoFAP-vedotin was administered daily. The combination of OncoFAP-vedotin with L19-IL2 exhibited a superior antitumor activity when compared with single agent treatments (4/4 CR, complete responses). (*B*) The tolerability of the different treatments as assessed by the evaluation of changes (%) in body weight during the experiment. ****$P < 0.0001$; **$P < 0.01$ (two-way ANOVA test, followed by Bonferroni posttest).

(serial dilution from 10^{-6} to 10^{-11} M, 1:2) in a total volume of 20 μL. Experiments were performed in triplicate, and the mean anisotropy values were fitted using Prism 7 (Y = Bottom + (Top − Bottom)/(1 + ((X^HillSlope)/(IC50^HillSlope)))). The value is defined as the concentration of inhibitor required to reduce the enzyme activity by 50% after addition of the substrate.

Transduction of Transmembrane hFAP in SK-RC-52 and HT-1080 Cells. The development of stable cell lines expressing FAP was performed using a second-generation lentiviral system based on the EF1-T2A vector (which was kindly provided by Renier Myburgh and Markus Manz) as previously described (25, 46). Briefly, HEK 293T cells (ATCC CRL-3216) were seeded overnight in a T75 tissue culture flask at a total density of 5 million cells using Dulbecco's Modified Eagle Medium (DMEM) media (Gibco) with 10% fetal bovine serum (FBS) (Gibco) and 1% antibiotic-antimycotic (Gibco). On day 1, cells were cotransfected with the transfer plasmid containing a cloned FAP transgene along with the envelope plasmid (pCAG-VSVG, Addgene, #35616; RRID: Addgene_35616) and the packaging plasmid (psPAX2, Addgene, #12260; Research Resource Identifier: Addgene_12260). The amino acid sequence for the full-length FAP is shown in *SI Appendix*, Fig. S5. jetPRIME (Polyplus-transfection SA) was added to improve the transfection efficiency according to the manufacturer recommendations. On day 2, the media was changed with a fresh one to enhance the viability. On day 3, the supernatant containing the virus was harvested, centrifuged at 400 × *g* for 5 min, and filtered through a 0.45 μm filter to remove cellular debris. The virus containing the FAP transgene was then concentrated using PEG-it Virus Precipitation Solution (System Biosciences) and stored at 4 °C. On day 5, the mixture was spun down at 1,500 × *g* for 30 min at 4 °C, and the supernatant was aspirated to pellet the virus particles. The pellet containing the virus particles was then resuspended in 100 μL DMEM media, aliquoted, and stored at −80 °C for future use.

For virus transduction, SK-RC-52 and HT-1080 cell lines were seeded at a density of 1 million cells in a 24-well plate using DMEM and Roswell Park Memorial Institute (RPMI) 1640, respectively. Next day, 10 μL of the virus aliquot and Polybrene (Santa Cruz Biotechnology, Inc.), to the final concentration of 8 μg/mL, were added to the cells. The plate was then centrifuged at 1,000 × *g* for 90 min at 32 °C to enhance the cellular uptake of the virus. In the following day, the media was changed, and cells were grown and expanded for 3 wk according to the general cell culture procedures. Finally, positive cells were sorted at the flow cytometry facility (BD FACSArial III) using FAP phycoerythrin-conjugated antibody (R&D Systems).

Cell Cultures. Upon thawing, SK-MEL-187, SK-RC-52.hFAP and SK-RC-52.wt cells were kept in culture in RPMI medium supplemented with FBS (10%) and Antibiotic-Antimycotic (AA, 1%) at 37 °C and 5% CO_2. For passaging, cells were detached using Trypsin-EDTA 0.05% when reaching 90% confluence and reseeded at a dilution of 1:4.

Upon thawing, HT-1080.hFAP and HT-1080.wt cells were kept in culture in DMEM supplemented with FBS (10%) and AA (1%) at 37 °C and 5% CO_2. For passaging, cells were detached using Trypsin-EDTA 0.05% when reaching 90% confluence and reseeded at a dilution of 1:4.

T cells were kept in culture in RPMI medium supplemented with FBS (10%), AA (1%), ultraglutamine (2 mM), and IL2 (Proleukin, Roche Diagnostic, 100 UI) at 37 °C and 5% CO_2. Cells were kept at a density of 10^6 cells per milliliter.

Internalization Studies by Confocal Microscopy Analysis. SK-RC-52.hFAP and SK-RC-52.wt cells were seeded into 4-well coverslip chamber plates (Sarstedt, Inc.) at a density of 10^4 cells per well in RPMI medium (1 mL, Invitrogen) supplemented with 10% fetal calf serum (FCS), AA, and Hepes (10 mM) and allowed to grow for 24 h under standard culture conditions. Hoechst 33342 nuclear dye (Invitrogen) was used to stain nuclear structures. The culture medium was replaced with fresh medium containing compound **2** (100 nM). Randomly selected colonies were imaged 1 h after incubation on a SP8 confocal microscope equipped with an AOBS device (Leica Microsystems).

HT-1080.hFAP and HT-1080.wt cells were seeded into 4-well coverslip chamber plates (Sarstedt, Inc.) at a density of 10^4 cells per well in DMEM (1 mL, Invitrogen) supplemented with 10% FCS, AA, and Hepes (10 mM) and allowed to grow for 24 h under standard culture conditions. Hoechst 33342 nuclear dye (Invitrogen) was used to stain nuclear structures. The culture medium was replaced with fresh medium containing compound **2** (100 nM). Randomly selected colonies were imaged 1 h after incubation on a SP8 confocal microscope equipped with an AOBS device (Leica Microsystems).

Flow Cytometry Analysis. SK-RC-52.hFAP, SK-RC-52.wt, HT-1080.hFAP, and HT-1080.wt were detached from culture plates using Accutase (Millipore), counted, and suspended to a final concentration of 1.5×10^6 cells/mL in a 1% vol/vol solution of FCS in phosphate-buffered saline (PBS), pH 7.4. Aliquots of 3×10^5 cells (200 μL) were spun down and resuspended in solutions of compound **2** (15 nM) in a 1% vol/vol solution of FCS in PBS, pH 7.4 (200 μL), and incubated on ice for 1 h. Cells were washed once with 200 μL 1% vol/vol solution of FCS in PBS, pH 7.4 (200 μL), spun down, resuspended in a 1% vol/vol solution of FCS in PBS, pH 7.4 (300 μL), and analyzed on a CytoFLEX Cytometer (Beckman Coulter). The raw data were processed with the FlowJo 10.4 software.

Animal Studies. All animal experiments were conducted in accordance with Swiss animal welfare laws and regulations under the license number ZH04/2018 granted by the Veterinäramt des Kantons Zürich.

Implantation of Subcutaneous Tumors. Tumor cells were grown to 80% confluence and detached with Trypsin-EDTA 0.05%. SK-RC-52.hFAP, SK-RC-52.wt, HT-1080.hFAP, and HT-1080.wt cells were resuspended in Hanks' Balanced Salt Solution medium. Alternatively, SK-MEL-187 was resuspended in a mixture of PBS:Matrigel (BD Biosciences; 8:2). Aliquots of 5 to 10×10^6 cells (100 to 150 μL of suspension) were injected subcutaneously in the right and/or left flanks of female athymic Balb/c AnNRj-Foxn1 mice (6 to 8 wk of age, Janvier).

Ex Vivo Experiments. Mice bearing subcutaneous SK-RC-52.hFAP or HT-1080.hFAP tumors were injected intravenously with compound **3** (40 nmol dissolved in sterile PBS, pH 7.4). Animals were euthanized by CO_2 asphyxiation 1 h after the intravenous injection, and the organs and the tumor were excised, snap frozen in optimal cutting temperature medium (Thermo Fisher Scientific), and stored at −80 °C. Cryostat sections (7 μm) were cut, and nuclei were stained with fluorescence mounting medium (Dako Omnis, Agilent). Images were obtained using an Axioskop 2 mot plus microscope (Zeiss) and analyzed by ImageJ 1.53 software.

Radiolabeling and Biodistribution Experiment with ^{177}Lu-OncoFAP. SK-RC-52.hFAP tumors were implanted into the right flank of female athymic Balb/c AnNRj-Foxn1 mice (6 to 8 wk of age) as described above and allowed to grow to an average volume of 250 mm^3. Mice were randomized ($n = 4$ per group) and injected intravenously with radiolabeled preparations of compound **4** (50, 125, 250, 500, or 1,000 nmol/kg; 0.5 to 2 MBq). Mice were euthanized 10 min, 1, 3, and 6 h after the injection by CO_2 asphyxiation, and organs were extracted, weighted, and radioactivity measured with a Packard Cobra Gamma Counter. Values are expressed as percent ID/g ± SD.

UniCAR T Cells In Vitro Killing Assay. UniCAR T cells and nontransduced T cells were purified from peripheral blood mononuclear cells as previously described (25) (all derived from the same healthy donor, Cerus, INTERCEPT Blood System) and were thawed and grown in a culture of 1×10^6 cells/mL in RPMI (Gibco). On day 0, SK-RC-52.hFAP, HT1080.hFAP, SK-RC-52.wt, and HT-1080.wt cell lines were harvested, and the membrane was stained using the PKH26 Red Fluorescent Cell Linker Kit for General Cell Membrane (Sigma-Aldrich) following manufacturer instructions. The cells were seeded in 96-well plates at a density of 30,000 cells/well and incubated overnight (37 °C, 5% CO_2). UniCAR T cells and nontransduced T cells were resuspended in 100 μL advanced RPMI (Gibco) containing different concentrations of bispecific adaptors and added on the various cell lines at a 1:1 target to effector cell ratio. As previously published, assay conditions, including UniCAR T cells and AAZ-fluorescein bispecific, targeting CAIX on SK-RC-52 cells were included as a positive control of the experiment (25). Nontransduced T cells and nontargeted fluorescein served as negative controls. After addition, the plate was spun down (400 g, 1 min, room temperature) and incubated for 24 h (37 °C, 5% CO_2). The killing rate was assessed via flow cytometry (*SI Appendix*, Fig. S6). The supernatant was transferred to a round bottom 96-well plate, and the wells were washed with 100 μL of PBS. Then, 50 μL Accutase (Millipore) was added to each well and incubated for 5 min at 37 °C to detach the target cells. The detached cells were added to the corresponding well of the round bottom 96-well plate. The plate was spun down (400 g, 5 min, room temperature) and flicked to remove the supernatant, and the pellets were resuspended in 150 μL FACS buffer and incubated for 30 min at 4 °C in the dark. The cells were spun down (400 g, 5 min, 4 °C). Immediately before measurement, the pellets were resuspended in a 1:10,000 dilution of the live/dead staining TOTO-3 Iodide (Thermo Fisher Scientific) in FACS buffer, strained (30 μm nylon mesh), and analyzed via flow cytometry (Cytoflex, Beckman Coulter). The flow cytometry data were analyzed using FlowJo software (Tree Star).

Therapy Experiment with OncoFAP-Vedotin. SK-RC-52.hFAP tumors were implanted into the right flank of female athymic Balb/c AnNRj-Foxn1 mice (6 to 8 wk of age) as described above and allowed to grow to an average volume of 100 mm^3. Mice were randomly assigned into therapy groups of four animals. Intravenous injections of OncoFAP-vedotin (compound **5**, 500 nmol/kg), L19-IL2 (2.5 mg/kg), or vehicles were performed with the schedules indicated in the text and in Fig. 6. Compound **5** was injected as sterile PBS solution with 2% dimethyl sulfoxide. L19-IL2 was injected in sterile formulation buffer (Philogen). Tumors were measured with an electronic caliper, and the animals were weighted daily. Tumor volume (mm^3) was calculated with the formula (long side, mm) × (short side, mm) × (short side, mm) × 0.5. Animals were euthanized when one or more termination criteria indicated by the experimental license were reached (e.g., weight loss > 15%). Prism 6 software (GraphPad Software) was used for data analysis (regular two-way ANOVA followed by Bonferroni test).

Data Availability. All study data are included in the article and/or *SI Appendix*.

ACKNOWLEDGMENTS. We thank Dr. Roberto De Luca and Fred Peissert for technical support during preparation of recombinant human and murine FAP. This project received funding from the European Research Council under the European Union's Horizon 2020 research and innovation program (Grant Agreement 670603) and under the Marie Skłodowska-Curie program (Grant Agreement 861316).

1. C. Kratochwil *et al*., 68Ga-FAPI PET/CT: Tracer uptake in 28 different kinds of cancer. *J. Nucl. Med.* **60**, 801–805 (2019).
2. O. C. Kulterer *et al*., A microdosing study with 99mTc-PHC-102 for the SPECT / CT imaging of primary and metastatic lesions in renal cell carcinoma patients. *J. Nucl. Med.* **62**, 360–365 (2020).
3. A. Kumar *et al*., Design of a small-molecule drug conjugate for prostate cancer targeted theranostics. *Bioconjug. Chem.* **27**, 1681–1689 (2016).
4. S. Cazzamalli *et al*., Enhanced therapeutic activity of non-internalizing small-molecule-drug conjugates targeting carbonic anhydrase IX in combination with targeted interleukin-2. *Clin. Cancer Res.* **24**, 3656–3667 (2018).
5. M. Srinivasarao, P. S. Low, Ligand-targeted drug delivery. *Chem. Rev.* **117**, 12133–12164 (2017).
6. J. Y. K. Lee *et al*., Folate receptor overexpression can be visualized in real time during pituitary adenoma endoscopic transsphenoidal surgery with near-infrared imaging. *J. Neurosurg.* **129**, 390–403 (2018).
7. C. E. S. Hoogstins *et al*., A novel tumor-specific agent for intraoperative near-infrared fluorescence imaging: A translational study in healthy volunteers and patients with ovarian cancer. *Clin. Cancer Res.* **22**, 2929–2938 (2016).
8. S. Cazzamalli, A. Dal Corso, F. Widmayer, D. Neri, Chemically defined antibody- and small molecule-drug conjugates for in vivo tumor targeting applications: A comparative analysis. *J. Am. Chem. Soc.* **140**, 1617–1621 (2018).
9. A. Smith *et al*., Unraveling the effect of immunogenicity on the PK/PD, efficacy, and safety of therapeutic proteins. *J. Immunol. Res.* **2016**, 2342187 (2016).
10. M. A. Firer, G. Gellerman, Targeted drug delivery for cancer therapy: The other side of antibodies. *J. Hematol. Oncol.* **5**, 70 (2012).
11. A. D. Herrera-Martínez *et al*., Targeted systemic treatment of neuroendocrine tumors: Current options and future perspectives. *Drugs* **79**, 21–42 (2019).
12. K. Rahbar, A. Afshar-Oromieh, H. Jadvar, H. Ahmadzadehfar, PSMA theranostics: Current status and future directions. *Mol. Imaging* **17**, 1536012118776068 (2018).
13. B. P. Mahon, M. A. Pinard, R. McKenna, Targeting carbonic anhydrase IX activity and expression. *Molecules* **20**, 2323–2348 (2015).
14. J. Strosberg *et al*.; NETTER-1 Trial Investigators, Phase 3 trial of ^{177}Lu-dotatate for midgut neuroendocrine tumors. *N. Engl. J. Med.* **376**, 125–135 (2017).
15. M. S. Hofman *et al*.; proPSMA Study Group Collaborators, Prostate-specific membrane antigen PET-CT in patients with high-risk prostate cancer before curative-intent surgery or radiotherapy (proPSMA): A prospective, randomised, multicentre study. *Lancet* **395**, 1208–1216 (2020).
16. P. Garin-Chesa, L. J. Old, W. J. Rettig, Cell surface glycoprotein of reactive stromal fibroblasts as a potential antibody target in human epithelial cancers. *Proc. Natl. Acad. Sci. U.S.A.* **87**, 7235–7239 (1990).
17. J. A. Tuxhorn *et al*., Reactive stroma in human prostate cancer: Induction of myofibroblast phenotype and extracellular matrix remodeling. *Clin. Cancer Res.* **8**, 2912–2923 (2002).
18. J. Niedermeyer *et al*., Targeted disruption of mouse fibroblast activation protein. *Mol. Cell. Biol.* **20**, 1089–1094 (2000).
19. W. N. Brennen, J. T. Isaacs, S. R. Denmeade, Rationale behind targeting fibroblast activation protein-expressing carcinoma-associated fibroblasts as a novel chemotherapeutic strategy. *Mol. Cancer Ther.* **11**, 257–266 (2012).
20. M. Syed *et al*., Fibroblast activation protein inhibitor (FAPI) PET for diagnostics and advanced targeted radiotherapy in head and neck cancers. *Eur. J. Nucl. Med. Mol. Imaging* **47**, 2836–2845 (2020).
21. C. Meyer *et al*., Radiation dosimetry and biodistribution of ^{68}Ga-FAPI-46 PET imaging in cancer patients. *J. Nucl. Med.* **61**, 1171–1177 (2020).
22. J. Calais, FAP: The next billion dollar nuclear theranostics target? *J. Nucl. Med.* **61**, 163–165 (2020).
23. J. R. Ballinger, Theranostic radiopharmaceuticals: Established agents in current use. *Br. J. Radiol.* **91**, 20170969 (2018).
24. Y. G. Lee *et al*., Use of a single CAR T cell and several bispecific adapters facilitates eradication of multiple antigenically different solid tumors. *Cancer Res.* **79**, 387–396 (2019).
25. C. Pellegrino *et al*., Impact of ligand size and conjugation chemistry on the performance of universal chimeric antigen receptor T-cells for tumor killing. *Bioconjug. Chem.* **31**, 1775–1783 (2020).
26. G. Bennett *et al*., MMAE delivery using the *bicycle* toxin conjugate BT5528. *Mol. Cancer Ther.* **19**, 1385–1394 (2020).

27. C. Zhuang *et al*., Small molecule-drug conjugates: A novel strategy for cancer-targeted treatment. *Eur. J. Med. Chem.* **163**, 883–895 (2019).
28. J. Millul *et al*., Immunotherapy with immunocytokines and PD-1 blockade enhances the anticancer activity of small molecule-drug conjugates targeting carbonic anhydrase IX. *Mol. Cancer Ther.* **20**, 512–522 (2020).
29. A. M. Scott *et al*., A phase I dose-escalation study of sibrotuzumab in patients with advanced or metastatic fibroblast activation protein-positive cancer. *Clin. Cancer Res.* **9**, 1639–1647 (2003).
30. S. Welt *et al*., Antibody targeting in metastatic colon cancer: A phase I study of monoclonal antibody F19 against a cell-surface protein of reactive tumor stromal fibroblasts. *J. Clin. Oncol.* **12**, 1193–1203 (1994).
31. R. D. Hofheinz *et al*., Stromal antigen targeting by a humanised monoclonal antibody: An early phase II trial of sibrotuzumab in patients with metastatic colorectal cancer. *Onkologie* **26**, 44–48 (2003).
32. P. Tanswell *et al*., Population pharmacokinetics of antifibroblast activation protein monoclonal antibody F19 in cancer patients. *Br. J. Clin. Pharmacol.* **51**, 177–180 (2001).
33. T. van der Geest *et al*., Liposomal treatment of experimental arthritis can be monitored noninvasively with a radiolabeled anti-fibroblast activation protein antibody. *J. Nucl. Med.* **58**, 151–155 (2017).
34. E. Ostermann *et al*., Effective immunoconjugate therapy in cancer models targeting a serine protease of tumor fibroblasts. *Clin. Cancer Res.* **14**, 4584–4592 (2008).
35. T. Lindner *et al*., Development of quinoline-based theranostic ligands for the targeting of fibroblast activation protein. *J. Nucl. Med.* **59**, 1415–1422 (2018).
36. M. Srinivasarao, C. V. Galliford, P. S. Low, Principles in the design of ligand-targeted cancer therapeutics and imaging agents. *Nat. Rev. Drug Discov.* **14**, 203–219 (2015).
37. N. Krall, J. Scheuermann, D. Neri, Small targeted cytotoxics: Current state and promises from DNA-encoded chemical libraries. *Angew. Chem. Int. Ed. Engl.* **52**, 1384–1402 (2013).
38. J. Wagner *et al*., Antitumor effects of CAR T cells redirected to the EDB splice variant of fibronectin. *Cancer Immunol. Res.* **9**, 279–290 (2020).
39. D. G. Song *et al*., A fully human chimeric antigen receptor with potent activity against cancer cells but reduced risk for off-tumor toxicity. *Oncotarget* **6**, 21533–21546 (2015).
40. K. L. Kahl, FDA approves first agent to treat locally advanced, metastatic urothelial cancer. *Oncology (Williston Park)* **34**, 11 (2020).
41. V. Milunović, K. Mišura Jakobac, M. Kursar, I. Mandac Rogulj, S. Ostojić Kolonić, FDA's and EMA's approval of brentuximab vedotin for advanced Hodgkin lymphoma: Another player in the town? *Eur. J. Haematol.* **103**, 145–151 (2019).
42. L. H. Sehn *et al*., Polatuzumab vedotin in relapsed or refractory diffuse large B-cell lymphoma. *J. Clin. Oncol.* **38**, 155–165 (2020).
43. M. Moschetta *et al*., Paclitaxel enhances therapeutic efficacy of the F8-IL2 immunocytokine to EDA-fibronectin-positive metastatic human melanoma xenografts. *Cancer Res.* **72**, 1814–1824 (2012).
44. R. W. Naumann *et al*., PRECEDENT: A randomized phase II trial comparing vintafolide (EC145) and pegylated liposomal doxorubicin (PLD) in combination versus PLD alone in patients with platinum-resistant ovarian cancer. *J. Clin. Oncol.* **31**, 4400–4406 (2013).
45. C. Wayua, J. Roy, K. S. Putt, P. S. Low, Selective tumor targeting of desacetyl vinblastine hydrazide and tubulysin B via conjugation to a cholecystokinin 2 receptor (CCK2R) ligand. *Mol. Pharm.* **12**, 2477–2483 (2015).
46. J. Mock, C. Pellegrino, D. Neri, A universal reporter cell line for bioactivity evaluation of engineered cytokine products. *Sci. Rep.* **10**, 3234 (2020).